



ELSEVIER

doi:10.1016/j.gca.2005.04.006

## Effects of temperature and transport conditions on calcite growth in the presence of Mg<sup>2+</sup>: Implications for paleothermometry

LAURA E. WASYLENKI,<sup>1</sup> PATRICIA M. DOVE,<sup>1,\*</sup> and JAMES J. DE YOREO<sup>2</sup><sup>1</sup>Department of Geosciences, Virginia Polytechnic Institute and State University, Blacksburg, VA 24061 USA<sup>2</sup>Department of Chemistry and Materials Science, Lawrence Livermore National Laboratory, Livermore, CA 94551 USA

(Received September 2, 2004; accepted in revised form April 7, 2005)

**Abstract**—This study links direct measurement of Mg-calcite growth kinetics with high-spatial-resolution analysis of Mg contents in experimental crystals, with particular attention to the effects of temperature on growth rate and reactant transport conditions on Mg distribution. In contrast to previous experiments on Mg partitioning into calcite, here the layer-growth mechanism was observed in situ and step speeds precisely measured with fluid cell atomic force microscopy over a range of temperatures, degrees of supersaturation, and solution Mg concentrations. Data collected from 15° to 30°C yield an activation energy for calcite precipitation of 33 kJ/mol for solutions with [Mg] = 5 × 10<sup>-5</sup> molal. Electron microprobe analyses of large hillocks grown at corresponding conditions demonstrate that Mg has a strong preference for incorporation at negative (acute) step edges, rather than at positive (obtuse) edges when growth rate is limited by surface reactions. This preference is reversed when growth is instead limited by diffusion of reactants through a boundary layer at the mineral-solution interface. These findings show that temperature is not the only strong control on the extent of Mg incorporation and distribution in calcite; transport conditions during mineral growth may also be a first-order factor governing the compositions of natural calcite samples. Copyright © 2005 Elsevier Ltd

### 1. INTRODUCTION

Calcium carbonates are the most abundant of the biogenic minerals, both in terms of quantities produced and widespread distributions across taxa (Lowenstam and Weiner, 1989). Marine algae, whose predominant mineral product is calcite, contain ~3 × 10<sup>15</sup> grams of carbon (Van Cappellen, 2003) and are thus a significant reservoir in the global cycle of carbon. Although much of the calcite dissolves in the water column or on the seafloor, some is permanently buried as sediment. This is the dominant mechanism by which CO<sub>2</sub> is removed from the atmosphere-ocean system to long-term storage in carbonate rocks (Bernier, 1990; Van Cappellen, 2003). Thus biogenic calcite plays a significant role in global climate control, and the response of the marine biomass to changing conditions is of great consequence.

During the growth of biogenic calcite, mineral crystals incorporate impurities, the concentrations of which appear to correlate with environmental conditions of growth for modern organisms (Chave, 1954; Dodd, 1965; Katz, 1973; Savin and Douglas, 1973; Füchtbauer and Hardie, 1976; Cronblad and Malmgren, 1981; Burton and Walter, 1987; Mucci, 1987; Oomori et al., 1987; Nürnberg et al., 1996; Rosenthal et al., 1997; Lea, 1999; Elderfield and Ganssen, 2000; Rosenthal et al., 2000; Toyofuku et al., 2000; Vander Putten et al., 2000). The potential for extracting growth conditions of the past from the chemical signatures recorded in fossil calcite samples motivates much current effort in paleoclimatology. However, correlations between trace element contents and physical or chemical conditions are not simple and display interspecies variations (Lea et al., 1999; Elderfield and Ganssen, 2000; Vander Putten et al., 2000). In many cases, multiple controls appear to be at work in

governing uptake of a given impurity. To reliably interpret trace element-based paleoproxies will require understanding, with some certainty, the growth behavior of calcite over the range of relevant conditions.

The trace element signatures in biogenic calcite samples are complex convolutions of externally imposed, physicochemical parameters and internally regulated, biologic controls. It is important to emphasize that, for paleoclimatology, the aim is to extract information about the former, despite the presence of the latter. Understanding the variations in calcite growth behavior and impurity uptake common to all calcite samples, regardless of biologic particulars, in response to changes in the environment is crucial to achieving the ultimate goal. Unless we know the thermodynamically and kinetically imposed changes in growth behavior that underlie the complex signatures found in nature, the quest to develop robust paleoproxy tools will be impeded.

#### 1.1. Magnesium

Of the minor elements found in calcite, magnesium is most abundant and displays some of the strongest correlations with growth conditions. A large number of investigations have shown that Mg contents in modern biogenic calcite samples are positively correlated with temperature (Chave, 1954; Dodd, 1965; Katz, 1973; Savin and Douglas, 1973; Füchtbauer and Hardie, 1976; Cronblad and Malmgren, 1981; Burton and Walter, 1987; Mucci, 1987; Oomori et al., 1987; Nürnberg et al., 1996; Rosenthal et al., 1997; Lea, 1999; Elderfield and Ganssen, 2000; Rosenthal et al., 2000; Toyofuku et al., 2000; Vander Putten et al., 2000). However, the relationship between temperature and Mg content in natural calcite appears not to be simple. Lea (2003) has noted that two of the most fundamental issues in development of magnesium paleothermometry are establishing robust calibrations of the Mg-thermometer and

\* Author to whom correspondence should be addressed (dove@vt.edu).

determining the influence of environmental factors other than temperature on Mg incorporation, such as pH, salinity, and seawater Mg/Ca. Indeed, a review of the literature reveals differences in the Mg-temperature relationship between species and sometimes between individual organisms of the same species (Lea et al., 1999; Elderfield and Ganssen, 2000; Vander Putten et al., 2000). In some studies, physicochemical parameters other than temperature appear to influence Mg contents as well as or even more strongly than growth temperature (Dodd, 1965; Lorens and Bender, 1980; Delaney et al., 1985; Nürnberg et al., 1996; Rosenthal et al., 1997; Lea, 1999; Vander Putten et al., 2000; Boyle and Erez, 2004). Other factors, such as the effects of gametogenesis and preferential dissolution of Mg-rich calcite, add to the difficulty of reconstructing paleotemperature records from fossil samples in a robust manner (Lea, 2003). Reliable interpretation of the Mg signatures in biogenic calcite samples will require more profound knowledge of how physical and chemical conditions in the environment affect mineral growth, especially with regard to the mechanisms by which growth conditions influence mineral composition, both during and after initial formation.

Even in the absence of complicating biologic factors, much remains to be understood about Mg and calcite growth in the inorganic system. Many studies of inorganic calcite growth have been published, and there is considerable disagreement as to which controls are important (Katz, 1973; Berner, 1975; Mucci and Morse, 1983; Burton and Walter, 1987; Mucci, 1987; Oomori et al., 1987; Morse and Bender, 1990; Paquette and Reeder, 1995; Rimstidt et al., 1998). Again, composition of inorganic calcite is believed to correlate positively with temperature to some extent (Katz, 1973; Füchtbauer and Hardie, 1976; Burton and Walter, 1987; Mucci, 1987; Oomori et al., 1987), but some studies report even stronger control of Mg contents by other parameters, such as solution Mg/Ca (Berner, 1975; Mucci and Morse, 1983).

## 1.2. Role of Kinetics and Rate-Controlling Mechanisms

Notably absent from the literature are definite conclusions regarding the relationships between temperature, growth rate, and impurity partitioning for Mg in calcite. Published experimental and modeling studies disagree on the importance of growth rate (Lahann and Siebert, 1982; Mucci and Morse, 1983; Berner, 1987; Watson, 1996; Rimstidt et al., 1998; Watson, 2004), and only a few bulk precipitation studies have systematically varied temperature (Katz, 1973; Burton and Walter, 1987; Mucci, 1987; Oomori et al., 1987; Arvidson and Mackenzie, 2000). Improved understanding of how growth rate varies with temperature, supersaturation state, and solution composition is still needed for deconvolution of the factors determining mineral composition.

Another factor that is not often considered in experimental or theoretical work is the rate-controlling mechanism, i.e., whether growth rate is limited by diffusive transport of chemical components to the mineral surface or by surface reactions such as dehydration, adsorption, and formation of lattice bonds (Morse, 1983; Lasaga, 1998). Variations in rate-controlling mechanism obviously cause variations in growth rate and boundary layer thickness and may thus affect the extent and nature of impurity incorporation during crystal growth. Reac-

tion rates involving growth or dissolution of calcite can be either transport- or surface-controlled (Morse, 1983; Lasaga, 1998). This distinction potentially has important ramifications for the Mg contents of natural calcite samples, especially where biomineralization in different organisms is concerned.

## 1.3. Objectives and Approach

Because of the ongoing uncertainties about how physical and chemical parameters affect calcite growth and composition and the critical importance of quantifying those relationships, we have investigated the response of calcite growth to temperature and solution chemistry with an approach similar to that of Davis et al. (2000), but over a range of temperatures common for natural waters. The aim of this work is to understand fundamentally the thermodynamic and kinetic effects of temperature, solution chemistry, and rate-controlling mechanism on calcite growth in the presence of Mg. The experiments presented in this paper contribute to knowledge of how externally imposed conditions affect calcite growth; once this baseline is established in the inorganic system, superimposed, biologic signatures can be more readily deconvolved from the complex observations made of natural variations in calcite Mg contents.

The approach used here includes kinetic measurements of calcite growth made in situ with atomic force microscopy (AFM). Use of the AFM enables direct observation of the near-equilibrium growth mechanism (monomolecular step propagation, see explanation in Section 2.1) at the scale appropriate for characterizing interactions between Mg and calcite steps. This is the first study of its kind to vary temperature systematically and precisely in this chemical system. It provides a critical link between nanoscale, kinetic measurements with a directly observed, near-equilibrium growth mechanism and chemical analysis of resulting solid calcite with high spatial resolution. A potentially important finding is that the distribution of Mg in calcite growth hillocks changes depending upon whether growth rate is controlled by diffusive transport at the mineral-solution boundary or by surface reactions at step edges. Because the rate-controlling mechanisms are as yet unknown for biologic mineralizing environments, this phenomenon may have significant consequences for interpreting biogenic Mg signatures.

## 2. EXPERIMENTAL AND ANALYTICAL METHODS

### 2.1. Near-Equilibrium Calcite Growth

As previously described (Paquette and Reeder, 1990; Gratz et al., 1993; Paquette and Reeder, 1995; Reeder, 1996; Teng et al., 1998), calcite precipitating from slightly supersaturated solution forms polygonal growth hillocks. Monomolecular steps emanate from spiral dislocations in the crystal lattice at the apices of the growth hillocks. The structure of the calcite lattice results in four hillock flanks with two geometrically distinct step types, one with obtuse angles between step risers and terraces (+) and the other with acute angles (-). Steps of these two types propagate at different speeds and are affected by impurities in different ways (Paquette and Reeder, 1995; Reeder, 1996; Davis et al., 2000; Wasylenki et al., 2005). Step speeds are proportional to growth rates; thus measurements of step speeds provide direct quantification of calcite growth kinetics.

## 2.2. Atomic Force Microscope Experiments

In these experiments calcite growth was observed and measured *in situ* with atomic force microscopy (AFM), using freshly cleaved seed crystals of calcite and a flow-through fluid cell, through which super-saturated growth solution was pumped. Methods were the same as those of Wasylenki et al. (2005) with the following exceptions. Growth solutions were held at the desired temperature by enclosing the last few centimeters of tubing within an assembly of brass plates. The plates contain fittings for circulating water and were heated or cooled by a water bath. Temperature, which ranged from 15° to 30°C, was monitored *in situ* with a Type T thermocouple placed in the exit port of the AFM fluid cell, a few millimeters from the sample. The temperature fluctuated briefly whenever the solution syringe was refilled, but we allowed the system to stabilize for several minutes before collecting data to assure steady state growth within 0.4°C of the temperature of interest. The pH of each solution was carefully adjusted to 8.50 by addition of several microliters of 1 M NaOH immediately before introduction to the fluid cell.

Growth was observed directly as monomolecular step flow in all cases, and step speeds were measured on steps emanating from spiral dislocation sources. Fluid flowed at 30 mL/h in all AFM experiments, and the residence time of solution in the fluid cell was ~6 s. As determined in previous experiments by Teng et al. (1998), this flow rate is sufficiently high for the rate-controlling mechanism to be surface reactions (Lasaga, 1998), rather than transport of chemical components to the mineral-solution interface. Teng et al. (1998) observed that below 25 mL/h, calcite growth rate was a function of fluid flow rate, but above 25 mL/h, fluid flow rate no longer affected step speed. The growth rates measured in our AFM experiments are therefore maxima, as compared with the rates that would be observed when diffusive transport limits growth rate.

While precision of AFM step speed measurements is extremely good (~0.1 nm/s), accuracy can be affected by a number of factors that are difficult to assess quantitatively. Thus we have conservatively estimated errors on all step speed measurements to be less than ± 2 nm/s when all sources of error are considered. Step speed measurements are made by continuously scanning a horizontal path across vertically oriented step edges, as in Teng et al. (2000). Friction between the O-ring, the fluid cell, and the sample puck could result in this horizontal scan being narrower than the nominal scan width by a few percent relative, leading to overestimated step speeds. A simple calibration for this effect was performed and applied to the data, but is likely not perfect in all cases, especially for features away from the center of the O-ring. Other possible sources of error, when growth is very slow and morphology is strongly affected by Mg, are the rough edges and curvature of steps; growth direction may be altered along some segments of a scalloped step-edge, but the method of calculating step speeds used here assumes straight edges migrating horizontally. Because step speed is proportional to the tangent of the angle subtended by steps in the AFM scans (see Teng et al., 2000), the reported speeds should be minimally affected for small deviations in step orientation. Sources of error that could result in anomalously slow step speeds include partial decarbonation of solution or nucleation of calcite in the tubing carrying solution to the sample. These errors and variations in solution composition due to weighing and pipetting are difficult to quantify; hence the conservative estimate of ± 2 nm/s applies to all measurements reported here.

## 2.3. Long-term Growth Experiments

The same solution recipes used for AFM were used to grow calcite hillocks as overgrowths that are thick enough for electron microprobe analysis of Mg contents. Two types of experiments were conducted. In the first, growth rate was limited by surface reactions, as in the AFM experiments; in the second, growth was limited by diffusive transport of components to the sample surface.

For surface-controlled experiments, seed crystals were cleaved as for AFM experiments and placed in Plexiglas replicas of the AFM fluid cell without cantilevers. Solutions of NaHCO<sub>3</sub>(s) and CaCl<sub>2</sub> · 2H<sub>2</sub>O(s) were loaded in parallel syringes and pumped continuously at 30 mL/h (2 × 15 mL/h) through the sample chambers for several hours to accelerate the process of hillock growth and coalescence until a few,

relatively large features remained on the surface. Following this, syringes were filled with NaHCO<sub>3</sub> and CaCl<sub>2</sub>+MgCl<sub>2</sub>+NaCl such that when these two components mixed, they replicated the recipes used in the AFM experiments. Solutions were not recycled.

Because the NaHCO<sub>3</sub> and chloride salt solutions did not mix until they reached the length of tubing between the syringe pump and sample chambers, it was not possible to adjust pH of the entire solution to exactly 8.50. Small, equal amounts of NaHCO<sub>3</sub> and chloride salt solutions were mixed before the experiment commenced, and the number of microliters of 1 M NaOH needed to achieve pH of 8.50 was noted. This amount of NaOH was scaled up and added to the remaining chloride salt stock. Before the syringes were reloaded with fresh bicarbonate solution and additional chloride salt stock, the pH of a mixture of equal amounts of the two solution components was checked and found to be within 0.05 of 8.50.

Samples and syringe pumps were kept in an incubator and temperature held within 0.5°C of the nominal experimental temperature, as measured with the same thermometer used for AFM experiments. Samples grew for 48–96 hours to precipitate overgrowths thick enough for electron microprobe analysis. At the conclusion of each experiment, samples were dried as quickly as possible under a stream of pressurized nitrogen to minimize evaporite precipitation on the surfaces. Crystals were then mounted on glass slides with double-sided carbon tape and carbon coated.

For diffusion-limited growth, seed crystals were placed within flasks of growth solution on a shaker table precessing at 120 rpm within an incubator. Flasks were filled with fresh solution every 12 hours for several days. Solution pH was adjusted to 8.50 with NaOH. Glass rods extending into the necks of the flasks displaced most of the air within the flasks to reduce decarbonation. At the conclusion of each experiment, samples were dried in nitrogen as above.

## 2.4. Solution Chemistry and Modeling of Supersaturation

Growth solutions supersaturated with respect to calcite were prepared from high-purity, reagent grade CaCl<sub>2</sub> · 2H<sub>2</sub>O, NaHCO<sub>3</sub>, MgCl<sub>2</sub> · 6H<sub>2</sub>O, and NaCl in distilled, deionized (18 MΩ) H<sub>2</sub>O. Supersaturation was defined as  $\sigma$ , where

$$\sigma = \ln \left( \frac{a_{\text{Ca}^{2+}} \times a_{\text{CO}_3^{2-}}}{K_{\text{sp}}} \right), \quad (1)$$

and  $K_{\text{sp}}$  is the equilibrium solubility product for pure calcite at the temperature of interest, calculated from the equations of Plummer and Busenberg (1982). Values of  $\sigma$  ranged from 0.20 to 1.20 (see Table 1). For each solution composition, the ratio of activities of Ca<sup>2+</sup> and CO<sub>3</sub><sup>2-</sup> was constrained to 1.0 and the pH to 8.50. NaCl concentration was 0.1 molal in all solutions; each solution had an ionic strength of 0.11. Concentrations of CaCl<sub>2</sub> and NaHCO<sub>3</sub> for each desired value of  $\sigma$  at each temperature were determined with The Geochemist's Workbench®, after substitution of equilibrium constants for calcite and related species from Plummer and Busenberg (1982) into the program's database. Iterative calculations for each value of  $\sigma$  at each temperature yielded the desired solution "recipes."

Mg was added to some solutions at concentrations of 2.5 × 10<sup>-5</sup> or 5.0 × 10<sup>-5</sup> molal as indicated in Table 1; values of  $\sigma$  reported in this paper are not corrected for addition of Mg. As each solution was prepared, its pH was adjusted to 8.50 by addition of several microliters of 1M NaOH. Experiments were run within 0.5°C of the nominal temperature. We assumed a closed system with respect to CO<sub>2</sub>; thus exposure to air was limited as much as possible during preparation and use of the growth solutions.

## 2.5. Electron Microprobe Analysis

Magnesium concentrations in calcite growth hillocks were measured using the Cameca SX-50 electron microprobe at Virginia Tech. Acceleration voltage was 10 kV. We attempted analyses at 5 kV, but could not sufficiently excite Mg X-rays; Mg concentrations in these samples are quite low. Analyses at 15 kV produced lower and more variable Mg concentrations than 10 kV, indicating beam penetration into the essentially Mg-free calcite seed crystal. Beam current at 10 kV was 20 na, chosen to optimize counts while minimizing damage to the sample

Table 1. Solution recipes used in growth experiments.\*

Temp (°C)	$\sigma$	$[\text{CaCl}_2] \times 10^4$	$[\text{NaHCO}_3] \times 10^3$	$a_{\text{Ca}^{2+}} \times 10^5$	$a_{\text{CO}_3^{2-}} \times 10^5$
15	0.50	2.62	9.90	7.81	7.84
15	0.60	2.77	10.42	8.22	8.24
15	0.70	2.93	10.90	8.66	8.61
15	0.80	3.10	11.50	9.12	9.08
15	0.90	3.27	12.10	9.57	9.54
15	1.00	3.46	12.80	10.06	10.08
15	1.10	3.65	13.40	10.56	10.55
15	1.20	3.86	14.15	11.09	11.13
20	0.40	2.37	8.05	7.25	7.24
20	0.50	2.50	8.46	7.62	7.61
20	0.60	2.64	8.92	8.01	8.01
20	0.70	2.79	9.37	8.43	8.41
20	0.80	2.95	9.87	8.87	8.85
20	0.90	3.11	10.38	9.30	9.30
20	1.00	3.29	10.92	9.79	9.78
20	1.20	3.67	12.13	10.8	10.8
23.5	0.23	2.14	6.54	6.68	6.38
23.5	0.33	2.26	6.87	7.03	6.70
23.5	0.43	2.39	7.23	7.40	7.05
23.5	0.53	2.52	7.59	7.77	7.39
23.5	0.63	2.66	7.98	8.17	7.77
23.5	0.73	2.81	8.42	8.59	8.19
23.5	0.83	2.96	8.86	9.01	8.61
23.5	0.93	3.13	9.32	9.48	9.05
30	0.30	2.05	5.80	6.47	6.45
30	0.40	2.16	6.11	6.80	6.79
30	0.50	2.28	6.42	7.14	7.14
30	0.60	2.41	6.76	7.52	7.51
30	0.70	2.54	7.10	7.89	7.88
30	0.80	2.69	7.47	8.32	8.29
30	1.00	3.00	8.26	9.19	9.15

\* Recipes calculated with Geochemist's Workbench<sup>®</sup> with solubility constants of Plummer and Busenberg (1982). All concentrations and activities are given in molal, and  $\sigma$  is defined as in the text. Every solution contained 0.1 molal NaCl, and pH was adjusted to 8.50 by addition of NaOH.  $[\text{MgCl}_2]$  was zero,  $2.5 \times 10^{-5}$  m, or  $5.0 \times 10^{-5}$  m, as indicated in Table 2 and figures.

surface. The Mg peak was measured for 70 or 80 s and positive and negative backgrounds for 20 s each for every point analyzed. On each analyzed hillock traverses or grids of points spaced 3 to 5 microns apart and totaling 40–100 microns across were analyzed to determine Mg contents of all four flanks of growth hillocks, thus yielding data with high spatial resolution that is easily correlated with reflected light photographs of growth features. Thus Mg concentrations were determined for the geometrically distinct flanks of calcite growth hillocks. The  $K\alpha$  line of Ca was measured simultaneously (20 s count time) for the purpose of checking analysis totals. Analyses were processed with the algorithms of Pouchou and Pichoir (1985). A seed crystal control grown in a solution with no added impurities was probed to confirm impurity concentrations in the calcite substrate below the detection limit of the microprobe.

### 3. EXPERIMENTAL RESULTS

#### 3.1. Step Speeds vs. Mg Concentration

We measured step speeds at temperatures from 15° to 30°C, with  $\sigma$  ranging from 0.2 to 1.2 and fluid  $[\text{Mg}]$  from 0 to  $5 \times 10^{-5}$  molal. Step speeds for all solutions for obtuse and acute steps are reported in Table 2.

In the figures we show subsets of the data, first at a constant temperature and then at constant fluid  $[\text{Mg}]$  to illustrate clearly the relationships between these variables and measured growth kinetics. Step speeds for all experiments conducted at 23.5°C are presented in Figure 1 as a function of fluid  $[\text{Mg}]$ . With one

exception, for each level of supersaturation, step speed decreases roughly linearly with increasing concentration of Mg in growth solution. Steps flowed 2 nm/s at  $\sigma = 0.23$  and did not flow perceptibly when  $5 \times 10^{-5}$  molal Mg was present. At  $\sigma = 0.53$ , step speed decreases from 8 nm/s without Mg to 5 nm/s with  $5 \times 10^{-5}$  molal Mg. At the highest  $\sigma$  investigated at this temperature, 0.93, step speed decreases from 16 to 14 nm/s over the same range of fluid  $[\text{Mg}]$ .

#### 3.2. The Effects of Supersaturation and Temperature

Figures 2a and 2b show step speeds as a function of  $\sigma$  at a constant fluid  $[\text{Mg}]$  of  $5 \times 10^{-5}$  molal for four different temperatures. Each single-temperature trend reflects a linear correlation between solution supersaturation and step speed for both obtuse and acute steps. In general, the slopes of these trends increase with increasing temperature; thus, the dependence of step speed on supersaturation is stronger at higher temperatures. Accordingly, step speeds at a given value of  $\sigma$  generally increase with increasing temperature, although, because the range of temperatures studied is small, in some cases the data overlap within the estimated  $\pm 2$  nm/s error. Steps migrate approximately twice as quickly at 30° as at 15°C. Obtuse step speeds measured in this study range from zero to 23 nm/s, while acute step rates range from zero to 11 nm/s.

Table 2. Step speeds for all atomic force microscopy experiments.

Temp (°C)	$\sigma$	[MgCl <sub>2</sub> ] (m)	v <sub>+</sub> (nm/sec)	v <sub>-</sub> (nm/sec)
15	0.5	5.0 × 10 <sup>-5</sup>	3.1	1.4
15	0.5	5.0 × 10 <sup>-5</sup>	2.8	1.2
15	0.6	5.0 × 10 <sup>-5</sup>	4.7	2.9
15	0.7	5.0 × 10 <sup>-5</sup>	7.0	3.4
15	0.8	5.0 × 10 <sup>-5</sup>	9.6	4.2
15	0.9	5.0 × 10 <sup>-5</sup>	11.3	4.4
15	1.0	5.0 × 10 <sup>-5</sup>	12.8	4.8
15	1.1	5.0 × 10 <sup>-5</sup>	16.8	5.5
15	1.2	5.0 × 10 <sup>-5</sup>	15.8	6.4
19.5	0.4	5.0 × 10 <sup>-5</sup>	2.0	1.3
19.5	0.6	5.0 × 10 <sup>-5</sup>	4.1	2.9
19.5	0.7	5.0 × 10 <sup>-5</sup>	4.4	3.6
19.5	0.8	5.0 × 10 <sup>-5</sup>	7.9	4.8
19.5	1.0	5.0 × 10 <sup>-5</sup>	11.2	5.1
19.5	1.2	5.0 × 10 <sup>-5</sup>	20.1	9.7
23.5	0.23	0	2.0	3.0
23.5	0.33	0	4.1	4.0
23.5	0.43	0	5.1	4.3
23.5	0.53	0	7.8	7.1
23.5	0.53	0	8.4	7.4
23.5	0.63	0	9.7	9.7
23.5	0.63	0	7.4	6.1
23.5	0.73	0	13.4	7.9
23.5	0.93	0	15.7	8.6
23.5	0.43	2.5 × 10 <sup>-5</sup>	5.6	5.3
23.5	0.53	2.5 × 10 <sup>-5</sup>	7.1	4.8
23.5	0.63	2.5 × 10 <sup>-5</sup>	7.5	7.3
23.5	0.73	2.5 × 10 <sup>-5</sup>	9.8	5.6
23.5	0.93	2.5 × 10 <sup>-5</sup>	15.0	6.4
23.5	0.33	5.0 × 10 <sup>-5</sup>	0.1	0.3
23.5	0.53	5.0 × 10 <sup>-5</sup>	5.3	3.8
23.5	0.63	5.0 × 10 <sup>-5</sup>	7.7	6.4
23.5	0.73	5.0 × 10 <sup>-5</sup>	9.6	5.8
23.5	0.83	5.0 × 10 <sup>-5</sup>	12.7	10.6
23.5	0.93	5.0 × 10 <sup>-5</sup>	13.7	8.1
30	0.3	5.0 × 10 <sup>-5</sup>	0.4	1.2
30	0.4	5.0 × 10 <sup>-5</sup>	4.4	2.8
30	0.6	5.0 × 10 <sup>-5</sup>	9.7	5.1
30	0.6	5.0 × 10 <sup>-5</sup>	10.3	4.4
30	0.6	5.0 × 10 <sup>-5</sup>	9.9	4.6
30	0.8	5.0 × 10 <sup>-5</sup>	20.7	7.8
30	1.0	5.0 × 10 <sup>-5</sup>	23.3	8.3

### 3.3. Concentrations and Distributions of Mg in Growth Hillocks

Contour plots of electron microprobe Mg data for surface-controlled growth are shown in Figures 3a and 3b. The solution for this experiment had  $\sigma = 0.7$  at 23.5°C with [Mg] = 5 × 10<sup>-5</sup> molal. The shapes and orientations of the growth hillocks are easily recognized in the compositional maps. Magnesium is more highly concentrated in acute-stepped (-) flanks than in obtuse-stepped (+) flanks. Steps with these two distinct geometries incorporated ~1100–1400 ppm Mg (0.45–0.58 mol%;  $K'_d = 0.024$ –0.031 =  $[X_{\text{Mg,calcite}}/X_{\text{Ca,calcite}}]/[m_{\text{Mg,sol'n}}/m_{\text{Ca,sol'n}}]$ ) and 650–850 ppm Mg (0.27–0.35 mol%;  $K'_d = 0.014$ –0.019), respectively. These values for  $K'_d$  are within the range defined by bulk inorganic calcite growth experiments (0.012–0.057; Katz, 1973; Füchtbauer and Hardie, 1976; Mucci and Morse, 1983; Mucci, 1987; Zhong and Mucci, 1989; Hartley and Mucci, 1996). In Figure 3b, where several growth features were packed closely together, Mg contents also appear to be elevated along zones of hillock convergence.

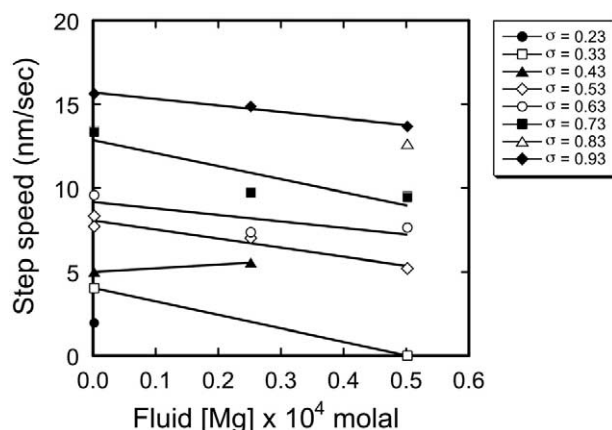


Fig. 1. Measurements of step speeds for obtuse steps, plotted as a function of fluid Mg concentration from 0 to 5 × 10<sup>-5</sup> molal, for eight levels of supersaturation. These trends show the linear decrease in step speeds with increasing [Mg]. Errors on step speed are conservatively estimated as ±2 nm/sec; see Section 2.2.

In contrast two experiments in which growth was limited by diffusive transport are shown in Figures 4a and 4b. The sample in Figure 4a was grown in solution with  $\sigma = 0.83$  at 23.5°C and [Mg] = 5 × 10<sup>-5</sup> molal, and for Figure 4b,  $\sigma = 0.83$  at 23.5°C and [Mg] = 1 × 10<sup>-4</sup> molal. In both experiments Mg was preferentially incorporated into obtuse-stepped (+) flanks of the growth hillocks (~1900 ppm or 0.78 mol% in Fig. 4a, ~1300 ppm or 0.53 mol% in Fig. 4b), in the opposite sense as observed for surface reaction-controlled growth. Acute flanks contain ~1400 ppm (0.58 mol%) in Figure 4a and 500 ppm (0.21 mol%) in Figure 4b. In addition, Mg concentrations are highest along the boundaries between obtuse and acute flanks, particularly in Figure 4a (~2400 ppm or 0.99 mol%, 2000 ppm or 0.82 mol% in Fig. 4b). Although shown with a color scale as for Figure 3, the measured concentrations in Figure 4 may have little quantitative value, as the supersaturated solutions in these experiments may have degassed or crystal nuclei may have formed during the 12 hours between solution changes (see Section 2.2), causing fluctuations in growth rate and carbonate speciation. Qualitatively, however, higher concentrations of Mg in obtuse-stepped flanks were observed in each of several similar experiments.

## 4. DISCUSSION

### 4.1. Inhibition of Calcite Growth by Magnesium

Previous work by Davis et al. (2000) and Dove et al. (2004) established the negative, linear relationship between calcite step speeds and Mg concentration in solution. Such linear decreases upon Mg addition indicate that Mg inhibits calcite growth through thermodynamic changes associated with incorporation of Mg<sup>2+</sup> in the calcite lattice. Because Mg<sup>2+</sup> is somewhat smaller than Ca<sup>2+</sup>, its incorporation causes lattice strain and thus a decrease in the negative enthalpy of calcite precipitation. For this reason, Mg-bearing calcite has greater solubility than pure calcite, so the effective supersaturation of growth solution is decreased upon addition of Mg (De Yoreo and Vekilov, 2003; Davis et al., 2004; Dove et al., 2004). The

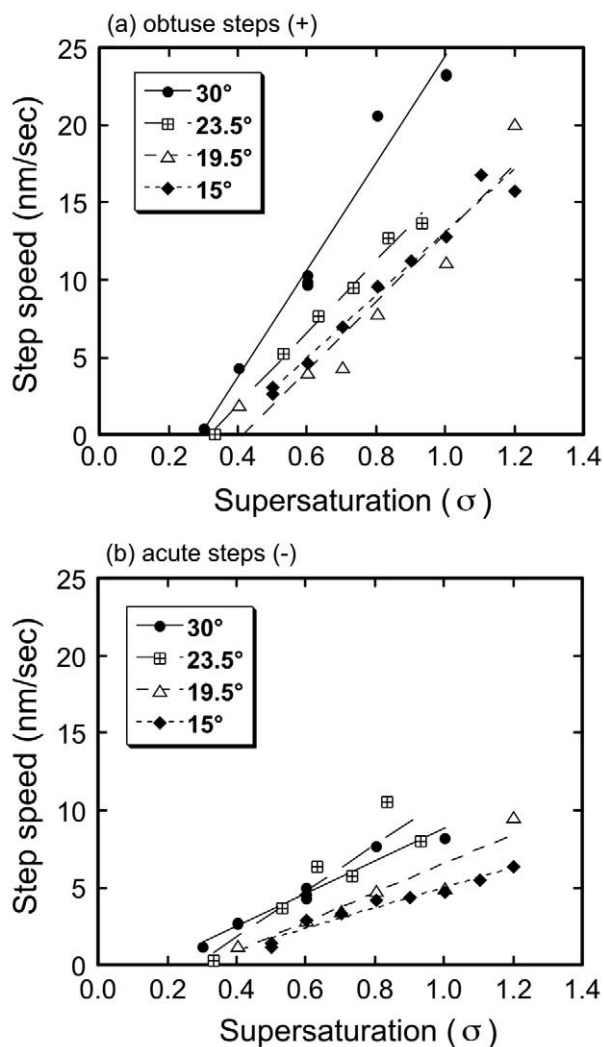


Fig. 2. Kinetic effect of temperature on growth rate at constant [Mg]: Step speeds for (a) obtuse and (b) acute steps versus degree of solution supersaturation ( $\sigma$ ) from 15°C to 30°C at [Mg] =  $5 \times 10^{-5}$  m. The thermodynamic effect of temperature on solution supersaturation has been taken into account by adjusting solution compositions accordingly; see Section 2.4 for definition of  $\sigma$  and discussion of Geochemist's Workbench<sup>®</sup> calculations. Lines represent best fits to the data for each temperature. These data are used to calculate activation energies for obtuse and acute step flow (see Fig. 5 and text).

current study confirms the nature of interactions between Mg and calcite growth surfaces for multiple temperatures and for lower extents of supersaturation and fluid [Mg] than previously investigated.

Our results also confirm a second phenomenon and extend it to new temperatures and solution compositions: the trends in Figure 2 do not extrapolate to step migration rates of zero at  $\sigma = 0$ , but at  $\sigma \sim 0.2$  to 0.3. One explanation for this is that the values of  $\sigma$  on the plot are for pure calcite, but the solid mineral being grown contains Mg. This Mg-calcite has a higher solubility, and the solution therefore has a lower effective supersaturation. We used estimates for the equilibrium activity of  $\text{Ca}^{2+}$  as a function of fluid [Mg] from Davis (2000) to determine that the magnitude of offset in  $\sigma$  for [Mg] =  $5 \times 10^{-5}$  m

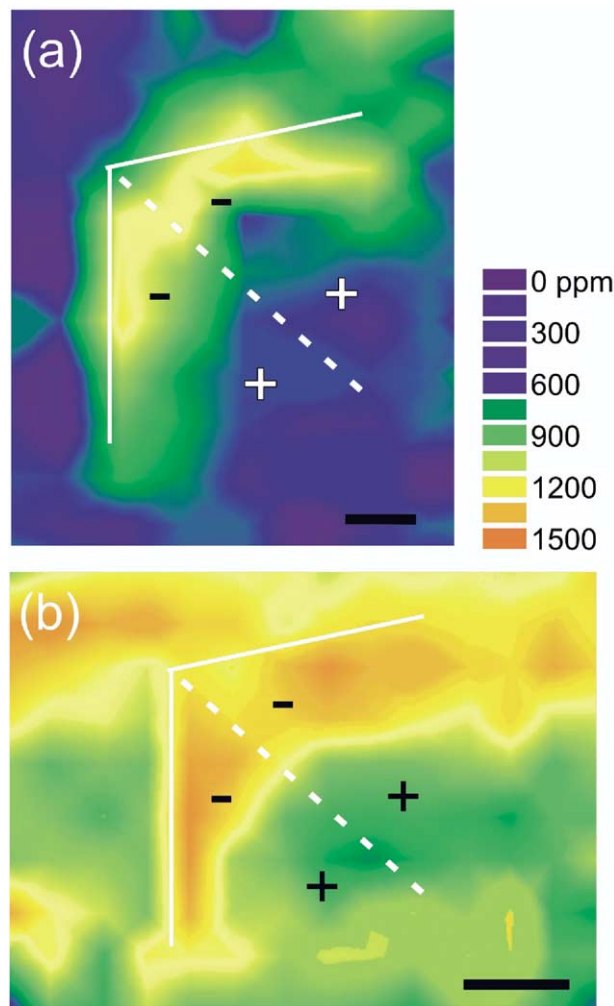


Fig. 3. Contour plots of electron microprobe analyses showing Mg content in calcite grown in surface reaction-limited conditions (vigorous fluid flow). (a) and (b) are two hillocks on the same sample surface. Solid white lines delineate the boundaries of the growth features, as identified in corresponding, reflected light photomicrographs of the sample surface. The dashed white lines represent the projection of the *c*-glide plane in calcite. The growth solution has  $\sigma = 0.7$  at 23.5°C with [Mg] =  $5 \times 10^{-5}$  molal. Scale bar is 10 microns.

is  $\sim 0.1$ . This is roughly half of the offset from zero that is apparent in Figure 2. A second possibility is that, because the smoothness of calcite step edges can inhibit growth at very low step speeds (Davis et al., 2000; Teng et al., 2000; De Yoreo and Vekilov, 2003), the trends in Figure 2 may curve slightly in a concave-upward sense as they approach speeds of zero, thus intersecting the ordinate axis at lower values of  $\sigma$ . Because of the difficulty of collecting accurate data at such low speeds, we have not attempted to capture that phenomenon in Figure 2. A third possibility is a consistent offset in supersaturation calculations from The Geochemist's Workbench<sup>®</sup>. Note that none of these considerations alters the relationships or interpretations of data discussed here.

Although we observed overall trends in growth kinetics that are similar to the earlier work, our step speeds are somewhat faster than those reported by Davis et al. (2000) for comparable

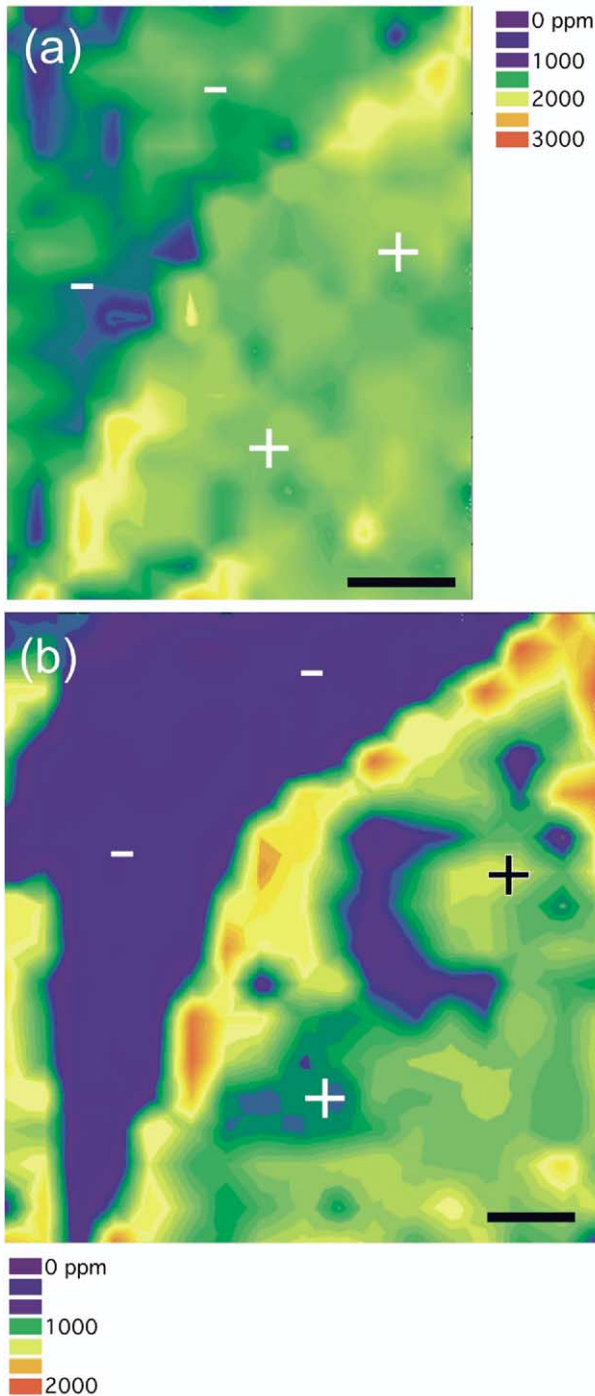


Fig. 4. Contour plots of electron microprobe analyses of Mg content in calcite grown in gently agitated growth solutions. Crystal growth in these cases was limited by diffusion of chemical components through a boundary layer at the mineral-solution interface. (a)  $\sigma = 0.43$  at 23.5°C,  $[\text{Mg}] = 5 \times 10^{-5}$  m, (b)  $\sigma = 0.83$  at 23.5°C,  $[\text{Mg}] = 1 \times 10^{-4}$  m. Scale bar is 10 microns.

conditions. One possible explanation for this discrepancy is a difference in identities and amounts of trace impurities in the chemical reagents or possibly in the deionized water used in these investigations. Another possibility is that temperatures in

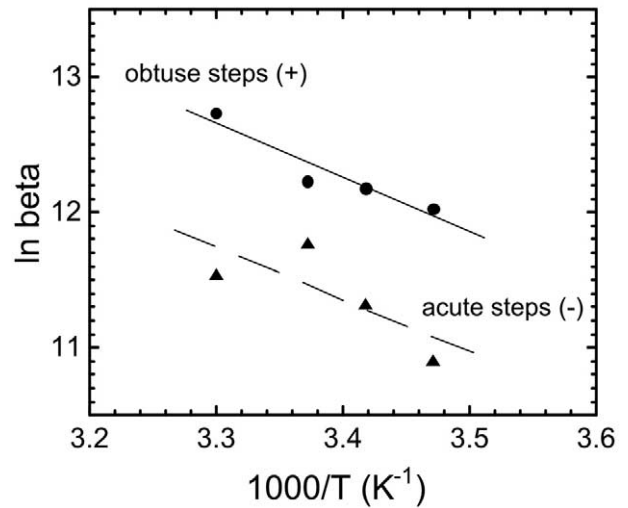


Fig. 5. Arrhenius diagram for calcite growth kinetics from 15° to 30°C, with fluid  $[\text{Mg}] = 5 \times 10^{-5}$  molal. The kinetic coefficient,  $\beta$ , is proportional to the slope of the trend in step speed versus  $[\text{Ca}_2^+] - [\text{Ca}_2^+]_{\text{eq}}$  for each temperature. Data for obtuse steps are shown; results for acute steps yield the same value for activation energy, 33 kJ/mol (0.34 eV/molecule).

the experiments here were more carefully monitored and controlled.

#### 4.2. Greater Sensitivity of Growth Rate to Supersaturation as Temperature Increases

The data in Figure 2 clearly show that, for a given degree of solution supersaturation, step migration rates for calcite are faster at warmer temperatures. Note that the decrease in solubility of calcite with increasing temperature is already taken into account by the values of  $\sigma$ ; the solution with  $\sigma = 1.0$  at 30°C has less  $\text{CaCl}_2$  and  $\text{NaHCO}_3$  than the  $\sigma = 1.0$  solution at 15°C because the value of  $K_{sp}$  (see Eqn. 1) is lower at 30°C. Thus the data, as presented, reflect kinetic effects of temperature on calcite growth, rather than thermodynamic effects.

Using these direct, quantitative measurements of step flow rates, we calculated activation energies for obtuse and acute steps according to the relations given in the following two equations. First,

$$v = \beta \omega ([\text{Ca}] - [\text{Ca}]_{\text{eq}}) \quad (2)$$

where  $v$  is step speed,  $\beta$  is the kinetic coefficient,  $\omega$  is the molecular volume of calcite,  $6.13 \times 10^{-23}$  cm<sup>3</sup>,  $[\text{Ca}]$  is the concentration of calcium in a given solution, and  $[\text{Ca}]_{\text{eq}}$  is the concentration of calcium in a solution in equilibrium with solid calcite. Thus, when the data are plotted as  $v$  vs.  $[\text{Ca}] - [\text{Ca}]_{\text{eq}}$ , the slope of each trend divided by  $\omega$  yields  $\beta$  for each temperature. Second,

$$\beta = e^{(-E_a/RT)}, \quad (3)$$

where  $E_a$  is the activation energy,  $R$  the gas constant, and  $T$  the Kelvin temperature. Arrhenius plots of  $\ln \beta$  vs. reciprocal temperature, shown in Figure 5, yield activation energies of  $33 \pm 3$  kJ/mol (0.34 eV/molecule) for obtuse and  $33 \pm 8$

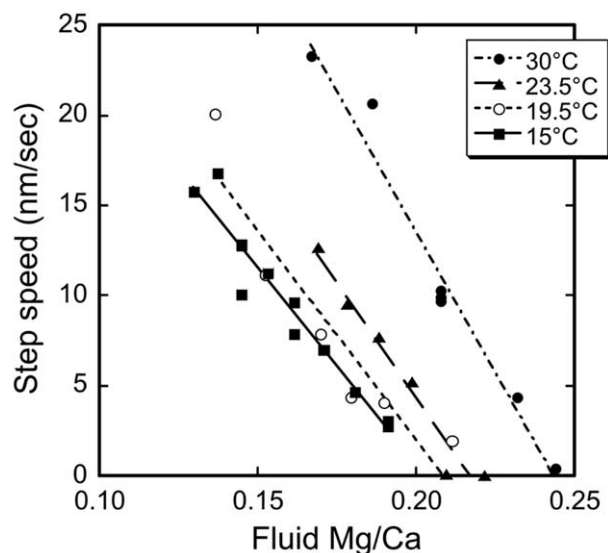


Fig. 6. Step speeds plotted versus solution Mg/Ca ratio (molar) for obtuse steps, demonstrating greater sensitivity of growth rate to solution chemistry with increasing temperature. Lines are best fits to the data at each temperature.

kJ/mol for acute step flow directions. This is in good agreement with values expected for surface reaction-limited growth of minerals (Lasaga, 1981), as well as the value of  $39.2 \pm 3.6$  kJ/mol for calcite determined in bulk precipitation studies by Kazmierczak et al. (1982), the activation energy of  $\text{KH}_2\text{PO}_4$  (31.8 kJ/mol; De Yoreo et al., 1997) and of barite ( $35 \pm 8$  kJ/mol; Bosbach and Wood, 2002).

Another consequence of the increase in slope with increasing temperature in Figure 2 is that, at higher temperatures, growth rate is more sensitive to changes in supersaturation. For example, at 30°C raising  $\sigma$  by 0.14 will result in a step speed increase of  $\sim 5$  nm/s for obtuse steps. For the same increase in step speed at 15°C,  $\sigma$  must be increased by 0.25. A linear fit to the data in Figure 2a yields the slope of the step speed- $\sigma$  dependence as a function of temperature:  $\delta v/\delta\sigma = 0.95T + 4.5$ , where  $T$  is in °C. A similar relation is evident if the data are cast as step speed vs. Mg/Ca ratio in solution, as in Figure 6; the change in Mg/Ca needed to cause a given change in growth rate decreases with increasing temperature. The slopes of the lines on this plot yield:  $\delta v/\delta(\text{Mg}/\text{Ca}) = -6.71T - 101.79$ , thus expressing quantitatively this relationship between calcite growth kinetics and solution chemistry.

### 4.3. Mg Fractionation

Our findings suggest that the distributions of Mg in calcite are highly dependent upon transport conditions. These results may have important implications for understanding trace element incorporation in calcite and biomineralization of Mg-bearing calcite. When crystal growth rate is controlled by the surface processes of adsorption, dehydration, and lattice incorporation, Mg is preferentially incorporated in acute-stepped (–) flanks of each growth hillock. Step-specific geometry and configuration of bonds formed when new growth units are added at step-edges are apparently key factors governing in-

corporation of Mg. The larger amount of Mg in acute-stepped flanks is the same sense of fractionation observed by Paquette and Reeder (1995), but their experiment (1) was likely dominated by diffusion-limited growth, as it was not vigorously stirred; and (2) contained significant concentrations of several impurities, including Sr, Ba, and Mn. Mg concentrations in our sample are substantially higher than those of Paquette and Reeder (1995), and the degree of fractionation between acute and obtuse steps is slightly higher, but direct, quantitative comparison is difficult, because of the differences just mentioned and the unknown concentration of Mg in the solution used in the other study.

A slight elevation in Mg concentration also occurs wherever two or more hillocks converge upon each other and where steps have “piled up” along ledges. We do not know exactly why this occurs, but speculate that it may be related to long residence times of adsorbed Mg species on the surface because of Mg’s strong binding properties (Stumm, 1992). We have not observed this phenomenon in our similar experiments with Sr (Wasylenki et al., 2005).

In contrast, when growth is limited by diffusion of chemical components to the mineral surface, more Mg is incorporated at obtuse step-edges than at acute step-edges. The compositional maps of growth hillocks produced under diffusion-limited conditions in Figure 4 are representative of many samples that displayed this behavior. From either the surface reaction-limited experiments or the transport-limited experiments alone, it is clear that the two types of molecular configurations at step-edges result in differential incorporation of Mg. In addition, the observed reversal in sense of the step-specific preference of Mg cations demonstrates that the particular effects of step-specific geometry on interactions between Mg and growing calcite vary significantly from one rate-controlling mechanism to the other.

Another finding from our diffusion-limited experiments is that the highest concentrations of Mg occur along the boundaries between obtuse- and acute-stepped flanks. The unique geometry of these “corners” is apparently better suited than other sites for accommodating the relatively small  $\text{Mg}^{2+}$  cations. This result supports the earlier hypothesis of Davis et al. (2004) that, in the presence of Mg, the slowest step speeds on calcite growth hillocks occur along the obtuse/acute boundaries because of high lattice strain at those sites. This increase in lattice strain, to which the morphologic changes observed by Davis et al. (2004) are attributed, is likely directly connected to preferential incorporation of  $\text{Mg}^{2+}$  as a substitute for  $\text{Ca}^{2+}$ . Recently, Han and Aizenberg (2003) documented macroscopic morphologic features in Mg-bearing calcite consistent with this model.

Since all of the incorporation experiments presented here were conducted at the same temperature, temperature is not the only control on Mg content in calcite. With the current results, it is not possible to quantify completely the relative contributions of temperature, solution chemistry, and growth-limiting conditions to calcite composition. However, these experiments do demonstrate clearly that impurity uptake is strongly affected by chemistry and surface structure at the mineral-solution interface and that these factors may influence the compositions of natural calcite.

## 5. IMPLICATIONS FOR BIOGENIC CALCITE

In concluding this paper, we suggest two potentially important implications of our findings. First, for any species that occurs across a wide range of temperatures in the ocean for which control of growth rate is critical to successful biomineral production, our results imply that organisms in warmer environments may need to exert stricter control on the chemistry of the mineralizing environment to control growth rates precisely. This may be most significant for organisms that build complex and faithfully reproduced structures comprising multiple single crystals with precise interlocking fits, such as the many spectacular varieties of coccolithophorids and foraminifera. This precision may also confer an ecological advantage, as detailed morphologic differences are now believed to regulate buoyancy, light and nutrient supply (Young and Henriksen, 2003). Control of growth rate may well be critical to these taxa. Changes in temperature are known to affect adversely the morphology and test size of *E. huxleyi* coccolithophorids cultured in the lab (Watabe and Wilbur, 1966), but the species examined in that study is abundant in proper form over a wide range of latitudes and temperatures in the modern oceans. Thus, while individual strains may suffer from imposed temperature changes, the species collectively possesses the capability to succeed over a wide range of conditions. If control of growth rate is needed for production of the elaborate morphologies seen in *E. huxleyi* and many others, then a biologic (genetic?) mechanism for strict control of chemistry in the mineralizing vesicles must be at work.

Our second set of experiments demonstrates that temperature is not the only strong control on the extent of Mg incorporation or on Mg distribution in calcite. The nature of the mineral-solution interface appears to have first-order importance, at least with regard to a diffusive boundary layer as the primary rate-limiting step in precipitation. What sorts of boundary layers or limiting conditions on growth occur during calcite production by different organisms, either externally or within some sort of delineated, interior spaces, is still unknown, but may be a fundamental control on impurity content of biogenic samples. In all likelihood, transport conditions in membrane-enclosed, biomineralizing microenvironments vary from one type of organism to another. The effects of these differences may help to account for interspecies differences in Mg uptake as a function of temperature, as observed by Lea et al. (1999), Elderfield and Ganssen (2000), and Vander Putten et al. (2000), among others. As knowledge of calcite biomineralization processes improves, the dependence of Mg distribution on step geometry and transport conditions may also provide a means to explain the variations in Mg concentration observed within individual organisms.

## 6. SUMMARY

We have presented two types of calcite growth experiments: one in which we directly measured step flow rates as a function of temperature and solution chemistry (with atomic force microscopy) and one that connects those measurements to chemical analysis of Mg distributions in calcite with high spatial resolution. The AFM experiments, conducted over a range of temperatures relevant to natural waters, quantify the effect of temperature on calcite growth rate and yield activation energies of 33 kJ/mol (0.34 eV/molecule) for both obtuse and acute step flow with fluid  $[Mg] = 5 \times 10^{-5}$  m. The experiments also show that the sensitivity of

growth rate to changes in solution supersaturation or Mg/Ca increases with increasing temperature. Samples analyzed for Mg by electron microprobe were grown in two ways to explore how transport conditions (i.e., the presence of a diffusive boundary layer) affect Mg uptake. Those samples for which growth was limited by diffusion incorporated more Mg at obtuse step-edges, in contrast to the result of Paquette and Reeder (1995). Mg was particularly highly concentrated along the obtuse/acute subsector boundaries, where step flow is slowest and lattice strain is likely highest (Davis et al., 2004). In an experiment where vigorous fluid flow made surface processes the limiting factor in growth, Mg partitioned more strongly into negative subsectors, demonstrating that transport conditions at the mineral-solution interface are an important control on the distribution of Mg in calcite grown from aqueous solution. This would suggest that when organisms employ vesicles and other compartments as an integral part of controlled biomineralization processes, signatures may be significantly overprinted by the transport and diffusion conditions of the local microenvironment.

*Acknowledgments*—The authors wish to thank E. B. Watson, A. Lutge, and an anonymous reviewer for kind and helpful reviews of the manuscript and D. Lea for editorial handling. This work was supported by NSF OCE-0083173 and DOE FG02-00ER15112.

*Associate editor:* D. Lea

## REFERENCES

- Arvidson R. S. and Mackenzie F. T. (2000) Temperature dependence of mineral precipitation rates along the  $\text{CaCO}_3$ - $\text{MgCO}_3$  join. *Aquatic Geochem.* **6**, 249–256.
- Berner R. A. (1975) The role of magnesium in the crystal growth of calcite and aragonite from sea water. *Geochim. Cosmochim. Acta* **39**, 489–504.
- Berner R. A. (1987) Equilibrium, kinetics and the precipitation of magnesian calcite from seawater. *Am. J. Sci.* **278**, 1475–1477.
- Berner R. A. (1990) Atmospheric carbon dioxide levels over Phanerozoic time. *Science* **249**, 1382–1386.
- Bosbach D. and Wood S. A. (2002) Linking molecular-scale barite precipitation mechanisms with macroscopic crystal growth rates. In *Water-rock interactions, ore deposits and environmental geochemistry; a tribute to David A. Crerar* (ed. R. Hellmann), Vol. 7, pp. 97–110. Houston, Texas: Geochemical Society.
- Boyle E. A. and Erez J. (2004) Does carbonate ion influence foraminiferal Mg/Ca? *EOS Trans. AGU* **84** (52), OS21G-01.
- Burton E. A. and Walter L. M. (1987) Relative precipitation rates of aragonite and Mg calcite from seawater: temperature or carbonate ion control? *Geology* **15**, 111–114.
- Chave K. E. (1954) Aspects of the biogeochemistry of magnesium: 1. Calcareous marine organisms. *J. Geol.* **62**, 266–283.
- Cronblad H. G. and Malmgren B. A. (1981) Climatically controlled variation of Sr and Mg in Quaternary planktonic foraminifera. *Nature* **291**, 61–64.
- Davis K. J. (2000) Magnesium as an impurity in calcite growth: thermodynamic and kinetic controls on biomineral formation. Masters thesis, Georgia Institute of Technology.
- Davis K. J., Dove P. M., and De Yoreo J. J. (2000) The role of  $\text{Mg}^{2+}$  as an impurity in calcite growth. *Science* **290**, 1134–1137.
- Davis K. J., Dove P. M., Wasylenki L. E., and De Yoreo J. J. (2004) Morphological consequences of differential  $\text{Mg}^{2+}$  incorporation at structurally distinct steps on calcite. *Am. Mineral.* **89**, 714–720.
- De Yoreo J. J., Land T. A. and Lee J. D. (1997) Limits on surface vicinality and growth rate due to hollow dislocation cores on KDP {101}. *Phys. Rev. Lett.* **78** (23), 4462–4465.
- De Yoreo J. J. and Vekilov P. G. (2003) Principles of crystal nucleation and growth. In *Biomineralization* (ed. P. M. Dove, J. J. De Yoreo and S. Weiner), Vol. 54, Mineralogical Society of America, Washington, D. C.

- Delaney M. L., Bé A. W. H., and Boyle E. A. (1985) Li, Sr, Mg, and Na in foraminiferal calcite shells from laboratory culture, sediment traps and sediment cores. *Geochim. Cosmochim. Acta* **49**, 1327–1341.
- Dodd J. R. (1965) Environmental control of strontium and magnesium in *Mytilus*. *Geochim. Cosmochim. Acta* **29** (5), 385–398.
- Dove P. M., Davis K. J., and De Yoreo J. J. (2004) Inhibition of CaCO<sub>3</sub> crystallization by small molecules: the magnesium example. In *Solid-fluid interfaces to nanostructural engineering* (ed. X. Y. Liu and J. J. De Yoreo), Vol. II, pp. 55–82. Boston: Kluwer/Plenum Academic Press.
- Elderfield H. and Ganssen G. (2000) Past temperature and  $\delta^{18}\text{O}$  of surface ocean waters inferred from foraminiferal Mg/Ca ratios. *Nature* **405**, 442–445.
- Füchtbauer H. and Hardie L. A. (1976) Experimentally determined homogeneous distribution coefficients for precipitated magnesian calcites: applications to marine carbonate cements. *Geol. Soc. Am. Abstr.* **8**, 87719.
- Gratz A. J., Hillner P. E., and Hansma P. K. (1993) Step dynamics and spiral growth on calcite. *Geochim. Cosmochim. Acta* **57** (2), 491–495.
- Han Y.-J. and Aizenberg J. (2003) Effect of magnesium ions on oriented growth of calcite on carboxylic acid functionalized self-assembled monolayer. *J. Amer. Chem. Soc.* **125** (14), 4032–4033.
- Hartley G. and Mucci A. (1996) The influence of P<sub>CO2</sub> on the partitioning of magnesium in calcite overgrowths precipitated from artificial seawater at 25°C and 1 atm total pressure. *Geochim. Cosmochim. Acta* **60**, 315–324.
- Katz A. (1973) The interaction of magnesium with calcite during crystal growth at 25–90°C and one atmosphere. *Geochim. Cosmochim. Acta* **37**, 1563–1586.
- Kazmierczak T. F., Tomson M. B., and Nancollas G. H. (1982) Crystal growth of calcium carbonate. A controlled composition kinetic study. *J. Phys. Chem.* **86**, 103–107.
- Lahann R. W. and Siebert R. M. (1982) A kinetic model for distribution coefficients and application to Mg-calcite. *Geochim. Cosmochim. Acta* **46**, 2229–2238.
- Lasaga A. C. (1981) Transition state theory. In *Kinetics of geochemical processes* (ed. A. C. Lasaga and R. J. Kirkpatrick), Vol. 8, pp. 135–169. Mineralogical Society of America, Washington, D. C.
- Lasaga A. C. (1998) Kinetic theory in the earth sciences. Princeton, New Jersey: Princeton University Press.
- Lea D. W. (1999) Trace elements in foraminiferal calcite. In *Modern Foraminifera* (ed. B. K.). Sen Gupta London: Chapman & Hall.
- Lea D. W. (2003) Elemental and isotopic proxies of past ocean temperatures. In *The oceans and marine geochemistry* (ed. H. Elderfield), Vol. 6, pp. 365–390. Oxford: Elsevier-Perigamon.
- Lea D. W., Mashiotta T. A. and Spero H. J. (1999) Controls on magnesium and strontium uptake in planktonic foraminifera determined by live culturing. *Geochim. Cosmochim. Acta* **63**, 2369–2379.
- Lorens R. N. and Bender M. L. (1980) The impact of solution chemistry on *Mytilus edulis* calcite and aragonite. *Geochim. Cosmochim. Acta* **44** (9), 1265–1278.
- Lowenstam H. A. and Weiner S. (1989) On biomineralization. New York: Oxford University Press.
- Morse J. W. (1983) The kinetics of calcium carbonate dissolution and precipitation. In *Carbonates: mineralogy and chemistry* (ed. R. J. Reeder), Vol. 11, pp. 227–264. Mineralogical Society of America, Washington, D. C.
- Morse J. W. and Bender M. L. (1990) Partition coefficients in calcite: examination of factors influencing the validity of experimental results and their application to natural systems. *Chem. Geol.* **82**, 265–277.
- Mucci A. (1987) Influence of temperature on the composition of magnesian calcite overgrowths precipitated from seawater. *Geochim. Cosmochim. Acta* **51**, 1977–1984.
- Mucci A. and Morse J. W. (1983) The incorporation of Mg<sup>2+</sup> and Sr<sup>2+</sup> into calcite overgrowths: influences of growth rate and solution composition. *Geochim. Cosmochim. Acta* **47**, 217–233.
- Nürnberg D., Bijma J., and Hemleben C. (1996) Assessing the reliability of magnesium in foraminiferal calcite as a proxy for water mass temperature. *Geochim. Cosmochim. Acta* **60** (5), 803–814.
- Oomori T., Kaneshima H., and Maezato Y. (1987) Distribution coefficient of Mg<sup>2+</sup> ions between calcite and solution at 10–50°C. *Mar. Chem.* **20**, 327–336.
- Paquette J. and Reeder R. J. (1990) New type of compositional zoning in calcite: insights into crystal-growth mechanisms. *Geol.* **18**, 1244–1247.
- Paquette J. and Reeder R. J. (1995) Relationship between surface structure, growth mechanism and trace element incorporation in calcite. *Geochim. Cosmochim. Acta* **59** (4), 735–749.
- Plummer L. N. and Busenberg E. (1982) The solubilities of calcite, aragonite and vaterite in CO<sub>2</sub>-H<sub>2</sub>O solutions between 0 and 90°C and an evaluation of the aqueous model for the system CaCO<sub>3</sub>-CO<sub>2</sub>-H<sub>2</sub>O. *Geochim. Cosmochim. Acta* **46**, 1011–1040.
- Pouchou J. L. and Pichoir F. (1985) “PAP”  $\Phi(\rho Z)$  procedure for improved quantitative microanalysis. In *Microbeam Analysis* (ed. J. T. Armstrong). San Francisco Press, Inc., San Francisco.
- Reeder R. J. (1996) Interaction of divalent cobalt, zinc, cadmium and barium with the calcite surface during layer growth. *Geochim. Cosmochim. Acta* **60** (9), 1543–1552.
- Rimstidt J. D., Balog A., and Webb J. (1998) Distribution of trace elements between carbonate minerals and aqueous solutions. *Geochim. Cosmochim. Acta* **62** (11), 1851–1863.
- Rosenthal Y., Boyle E. A., and Slowey N. (1997) Temperature control on the incorporation of magnesium, strontium, fluorine and cadmium into benthic foraminiferal shells from Little Bahama Bank: prospects for thermocline paleoceanography. *Geochim. Cosmochim. Acta* **61**, 3633–3643.
- Rosenthal Y., Lohmann G. P., Lohmann K. C., and Sherrell R. M. (2000) Incorporation and preservation of Mg in *Globigerinoides sacculifer*: implications for reconstructing the temperature and <sup>18</sup>O/<sup>16</sup>O of seawater. *Paleoceanogr.* **15** (1), 135–145.
- Savin S. M. and Douglas R. G. (1973) Stable isotope and magnesium geochemistry of recent planktonic foraminifera from the south Pacific. *GSA Bull.* **84**, 2327–2342.
- Stumm W. (1992) Chemistry of the solid-water interface: processes at the mineral-water and particle-water interface in natural systems. John Wiley & Sons, Inc., New York.
- Teng H. H., Dove P. M. and De Yoreo J. J. (2000) Kinetics of calcite growth: surface processes and relationships to macroscopic rate laws. *Geochim. Cosmochim. Acta* **64** (13), 2255–2266.
- Teng H. H., Dove P. M., Orme C. A., and De Yoreo J. J. (1998) Thermodynamics of calcite growth: baseline for understanding biomineral formation. *Science* **282**, 724–727.
- Toyofuku T., Kitazato H., Kawahata H., Tsuchiya M., and Nohara M. (2000) Evaluation of Mg/Ca thermometry in foraminifera: comparison of experimental results and measurements in nature. *Paleoceanogr.* **15** (4), 456–464.
- Van Cappellen P. (2003) Biomineralization and global biogeochemical cycles. In *Biomineralization* (ed. P. M. Dove, J. J. De Yoreo and S. Weiner), Vol. 54. Mineralogical Society of America, Washington, D. C.
- Vander Putten E., Dehairs F., Keppens E., and Baeyens W. (2000) High resolution distribution of trace elements in the calcite shell layer of modern *Mytilus edulis*: environmental and biological controls. *Geochim. Cosmochim. Acta* **64** (6), 997–1011.
- Wasylenki L. E., Dove P. M., and De Yoreo J. J. (2005) Nanoscale effects of strontium on calcite growth: an *in situ* AFM study in the absence of vital effects. *Geochim. Cosmochim. Acta* **69**, 3017–3027.
- Watabe N. and Wilbur K. M. (1966) Effects of temperature on growth, calcification and coccolith form in *Coccolithus huxleyi* (*Coccolithineae*). *Limnol. Oceanogr.* **11** (4), 567–575.
- Watson E. B. (1996) Surface enrichment and trace-element uptaking during crystal growth. *Geochim. Cosmochim. Acta* **60**, 5013–5020.
- Watson E. B. (2004) A conceptual model for near-surface kinetic controls on the trace-element and stable isotope composition of abiogenic calcite crystals. *Geochim. Cosmochim. Acta* **68** (7), 1473–1488.
- Young, J. R. and Henriksen, K. (2003) Biomineralization within vesicles: the calcite of coccoliths. In *Biomineralization* (ed. P. M. Dove, J. J. De Yoreo and S. Weiner), Vol. 54. Mineralogical Society of America, Washington, D. C.
- Zhong S. and Mucci A. (1989) Partitioning of rare earth elements (REE's) between calcite and seawater solutions at 25°C and 1 atm and high dissolved REE concentrations. *Geochim. Cosmochim. Acta* **59**, 443–453.